Single-particle dynamics in particle storage rings with integrable polynomial factorization maps

Jicong Shi and Piriya Suwannakoon
Department of Physics and Astronomy, The University of Kansas, Lawrence, Kansas 66045
(Received 30 June 1998)

A six-dimensional symplectic tracking code based on the concept of integrable polynomial factorization (IPF) maps has been developed for the study of beam dynamics in large storage rings. To examine the accuracy of the IPF maps, comparison studies on beam dynamics between the IPF maps and the original system have been conducted with two sample lattices: a lattice containing one sextupole kick that is otherwise linear and the LHC (Large Hadron Collider) collision lattice. It was found that the errors in the nth-order IPF map scale as the $(n+1)$th power of phase-space amplitude. As the order of the map is increased, the difference between the original system and its IPF map can thus be reduced to be as small as desired. A study of phase-space portraits showed that the IPF map precisely reproduces the resonance structure of the original system even in the phase-space region where the system is quite nonlinear. The tracking study for the LHC showed that the IPF map accurately predicts the same dynamic aperture as does element-by-element tracking. Our results suggest that the IPF map is a reliable model for the study of long-term behavior of beam particles in large storage rings. [S1063-651X(98)02112-6]

PACS number(s): 29.20.−c, 29.27.−a, 05.45.+b, 03.20.+i

I. INTRODUCTION

In large storage rings, charged-particle beams are required to circulate for many hours in the presence of nonlinear perturbations of multipole errors in magnets. Extensive computer simulations are necessary to investigate the long-term stabilities of particle motions. To good approximation, particularly for hadron storage rings, the orbits of charged particles are described by Hamiltonian flows and, therefore, a symplectic tracking is required for such studies.

Over the past decade, the use of one-turn maps with the aid of Lie algebra and automatic differentiation (differential algebra) has attracted wide attention in the study of nonlinear beam dynamics in large storage rings [1–11]. Map methods have the advantage of substantial computational as well as conceptual simplification and could provide more realistic models of actual machines than those provided by conventional methods. The major obstacle in the application of maps to the study of the long-term stability of particle motions is, however, the construction of symplectic maps which can not only model actual machines with desired accuracy but also be directly used for tracking without breaking the symplecticity of systems. Maps in the form of Lie transformations with Dragt-Finn factorization, for example, are guaranteed to be symplectic, but they generally cannot be used for tracking directly [4]. Truncated expansions of one-turn maps, on the other hand, can be directly used for tracking, but the truncation inevitably violates the symplectic nature of systems and consequently leads to spurious effects if the maps are used to study the long-term stability [5]. One way to construct a symplectic map for a storage ring is adding small correction terms to a truncated one-turn map so that it can be converted into a symplectic map. Methods have been developed for the construction of such a symplectic map including the use of generating function [4,6], Cremona maps (Jolt factorization, kick factorization) [4,7,8], and integrable polynomial factorization (IPF) maps [9–11].

An IPF map is composed of Lie transformations associated with integrable polynomials [9–11]. It is exactly symplectic and can be directly used for tracking. Recently, a six-dimensional tracking code based on the concept of the IPF map has been developed for the study of the long-term behavior of beam particles in large storage rings. In this paper a test of the IPF map on the four-dimensional Hénon map and the Large Hadron Collider (LHC) collision lattice are reported. Comparison studies between the IPF map and the original system showed that the IPF map can precisely describe the beam dynamics. The long-term tracking study of the LHC showed that the IPF map predicted the same dynamic aperture as does element-by-element tracking.

This paper is organized as follows. In Sec. II we briefly recall the concept of the IPF map. The comparison study between the IPF map and the original system for the cases of the Hénon map and the LHC are reported in Secs. III and IV, respectively. Section V contains a summary.

II. INTEGRABLE POLYNOMIAL FACTORIZATION MAP

At any ''checkpoint'' of an accelerator, motions of particles can be described mathematically by a six-dimensional symplectic one-turn map

$$\mathbf{Z}' = \mathcal{M}\mathbf{Z}, \tag{1}$$

where $\mathbf{Z}=(x,p_x,y,p_y,z,p_z)$ is a phase-space vector and $\mathcal{M}$ is, in general, a nonlinear functional operator. Because we are usually not interested in transformations that simply translate the origin in phase space, only maps that map the origin to itself ($\mathbf{Z}=\mathbf{0}$ is the closed orbit) are considered. Within its analytic domain, $\mathcal{M}$ can be expanded in a power series of $\mathbf{Z}$,

$$\mathbf{Z}' = \sum_{i=1}^{n} \mathbf{U}_i(\mathbf{Z}) + \boldsymbol{\epsilon}(n+1), \tag{2}$$

where $\mathbf{U}_i(\mathbf{Z})$ is a vectorial homogeneous polynomial in $\mathbf{Z}$ of degree i and $\epsilon(n+1)$ represents a remainder series consisting of terms higher than the nth order. Truncating the expansion in Eq. (2) at the Nth order results in an nth-order Taylor map. Since such truncation inevitably violates the symplectic condition, the Taylor map typically produces spurious damping or growth when used to study the long-term behavior of trajectories. In order to use a one-turn map to study the long-term stability, the Taylor map has thus to be replaced by a symplectic map that can be easy to evaluate exactly and whose effect is identical to that of the Taylor map through some order. It has been shown that such a symplectic map can be constructed, by using the method of automatic differentiation, as a product of Lie transformations in the form of IPF [10],

$$\mathbf{Z}' = \mathcal{R} \prod_{i=3}^{n+1} \left[\prod_{k=1}^{N_g(i)} \exp(:g_i^{(k)}:) \right] \mathbf{Z} + \epsilon(n+1), \tag{3}$$

where $\mathcal{R}$ denotes a linear transformation corresponding to the linear betatron oscillation, $:g_i^{(k)}:$ represents the Lie operator associated with the kth integrable polynomial $g_i^{(k)}(\mathbf{Z})$ of degree i, and $N_g(i)$ is the number of integrable polynomials of degree i. In the six-dimensional phase space, $N_g(i)=8,\ 20,\ 42$, or 77 for $i=3,\ 4,\ 5$, or 6. Because a Lie transformation associated with an integrable polynomial can be expressed as an explicit function of $\mathbf{Z}$, $\exp(:g_i^{(k)}:)\mathbf{Z}$ can be easily evaluated exactly. Reference [9] contains the details of method for constructing integrable polynomials. Neglecting the remainder term $\epsilon(n+1)$ in Eq. (3), the nth-order IPF map is obtained as

$$\mathcal{M}_n = \mathcal{R} \prod_{i=3}^{n+1} \left[\prod_{k=1}^{N_g(i)} \exp(:g_i^{(k)}:) \right]. \tag{4}$$

The fifth-order IPF map is, for example, composed of 147 explicit maps all of which can be iterated directly.

Recently we have developed a six-dimensional tracking code (in object-oriented C++) based on the concept of IPF maps for studying beam dynamics in particle storage rings. To examine the validity of the approximation involved in the IPF, the accuracy of IPF maps will be studied with the following two sample lattices.

III. FOUR-DIMENSIONAL HÉNON MAP

The first example is a ring with one sextuple kick that is otherwise linear. In this case, the exact one-turn map can be written as a four-dimensional Hénon map

$$\mathcal{M}: \begin{cases} x' = \cos(2\pi\nu_x)x + \sin(2\pi\nu_x)[p_x - (x^2 - y^2)] \\ p_x' = -\sin(2\pi\nu_x)x + \cos(2\pi\nu_x)[p_x - (x^2 - y^2)] \\ y' = \cos(2\pi\nu_y)y + \sin(2\pi\nu_y)(p_y + 2xy) \\ p_y' = -\sin(2\pi\nu_y)y + \cos(2\pi\nu_y)(p_y + 2xy), \end{cases} \tag{5}$$

where ν_x and ν_y are linear tunes of the betatron oscillation. IPF maps of order 2 to 5 were constructed as approximations for the Hénon map by using our computer code. To examine the long-term behavior of the IPF maps, we repeatedly iterate the Hénon map and its IPF approximations on various initial conditions and compare the phase-space plots. Figures 1 and 2 display two-dimensional projections of the phase space of the Hénon map and its fifth-order IPF map, respectively, for $\nu_x=0.2114$ and $\nu_y=0.2314$. Comparison of Figs. 1 and 2 shows that within the phase-space region of interest the difference in phase space between the IPF map and its original system is invisible. To further examine the resonance structure of the IPF map, the phase-space portrait of the horizontal motion ($y=p_y=0$) was plotted in Fig. 3, which shows that the IPF map precisely reproduces the resonance structure of the original system even in the region where the system is quite nonlinear.

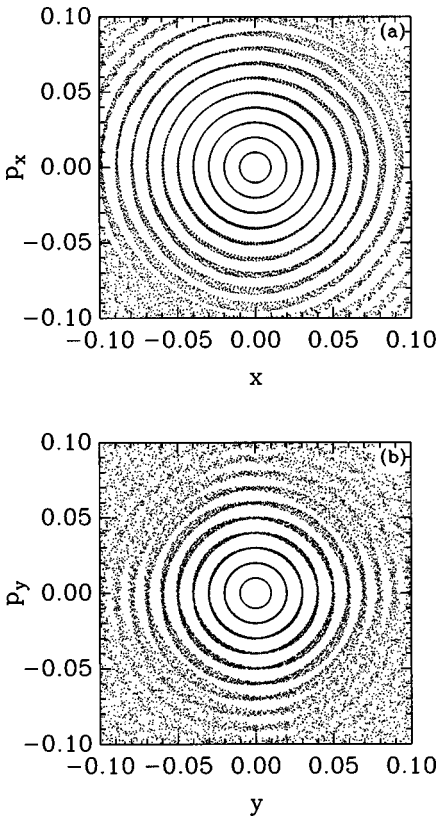

FIG. 1. Phase-space projection on (a) x-p_x plane and (b) y-p_y plane of four-dimensional Hénon map. $\nu_x=0.2114$ and $\nu_y=0.2314$.

To estimate errors in the approximation of the IPF, we computed the relative error defined by [4]

$$\delta_n(\mathbf{Z}) = ||\mathcal{M}\mathbf{Z} - \mathcal{M}_n\mathbf{Z}||/||\mathbf{Z}||, \tag{6}$$

where $||\cdot||$ denotes the Euclidean norm of the phase space and subscript n denotes the order of the IPF map. In Fig. 4, $\delta_2(\mathbf{Z})$ and $\delta_5(\mathbf{Z})$ were plotted in action-angle variables defined by $(x,p_x,y,p_y) = (I_x^{1/2}\cos\phi_x, I_x^{1/2}\sin\phi_x, I_y^{1/2}\cos\phi_y, I_y^{1/2}\sin\phi_y)$. As the order of the IPF map increases, the error is substantially reduced. To examine the dependence of the error on the order of the IPF map and on the phase-space amplitudes, we define the maximal error at a given amplitude $I_x=I_y=I$ as

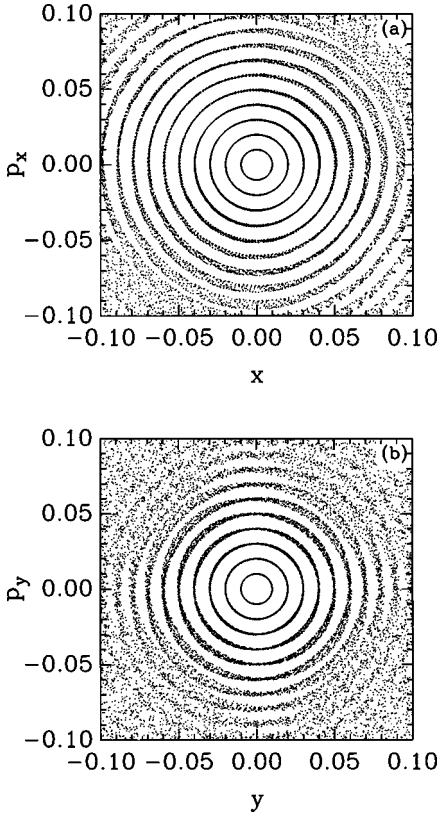

FIG. 2. Phase-space projection on (a) x-p_x plane and (b) y-p_y plane of the fifth-order IPF approximation of the four-dimensional Hénon map. $\nu_x = 0.2114$ and $\nu_y = 0.2314$.

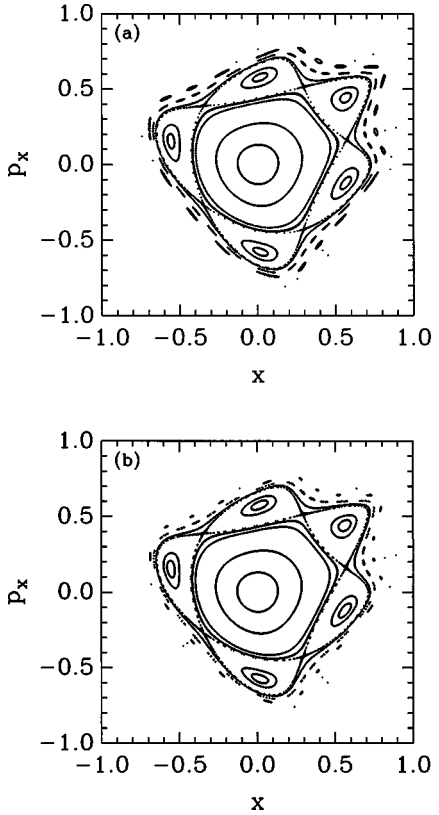

FIG. 3. Phase-space portrait of the horizontal motion ($y = p_y = 0$) of (a) the Hénon map and (b) the fifth-order IPF approximation of the Hénon map. $\nu_x = 0.2114$.

$$\delta_{\max}(I) = \max_{(\phi_x, \phi_y)} [\delta_n(\mathbf{Z})]. \tag{7}$$

In Figs. 5 and 6 $\delta_{\max}$ is plotted as a function of I and n, respectively. The error in the IPF map is found to increase with the phase-space amplitude (see Fig. 5) but such increase can be suppressed by increasing the order of the IPF map (see Fig. 6). In the inset of Fig. 5, $\log_{10}(\delta_{\max})$ is plotted as a function of $\log_{10}(I)$, which shows a power-law dependence of $\delta_{\max}$ on I. From the slopes of $\log_{10}(\delta_{\max})$-$\log_{10}(I)$ plots we found that $\delta_{\max}$ of the nth-order IPF map is proportional to I^n, which indicates that the difference between the exact system and its nth-order IPF map scales as $||\mathbf{Z}||^{n+1}$. Within the phase-space region of interest, the difference between the original system and its IPF approximation can therefore be reduced as small as desired.

It should be noted that even though all data discussed here are from the case of $\nu_x = 0.2114$ and $\nu_y = 0.2314$, other cases of different linear tunes were also studied and the results were found to be similar.

IV. THE LHC COLLISION LATTICE

The Large Hadron Collider to be built at CERN has four interaction regions (IRs) of which two are high luminosity IRs ($\beta^* = 0.5$ m) [12]. During collisions, the beam dynamics is dominated by the field errors of high gradient quadrupoles (HGQ) of inner triplets in the IRs because of large β functions ($\beta_{\max} \sim 4700$ m) and the beam separation in the triplets. In this study we only consider the random field errors in the HGQ. All systematic errors as well as the dipole and skew quadrupole component of random field error are taken to be zero. The random multipole components up to the fifth order are included and chosen with Gaussian distributions centered at zero and truncated at $\pm 3\sigma_{b_n}$ or $\pm 3\sigma_{a_n}$ where σ_{b_n} and σ_{a_n} are the rms value of the nth-order normal and skew multipole coefficient, respectively. In this study we used the error table of the Fermilab design of the HGQ [13]. The magnetic field errors in each HGQ are represented by a set of thin-lens multipole kicks, in which each magnet is sliced. In this study we used seven kicks in each HGQ including kicks at both ends. In order to minimize beam-beam effects, two counter-rotating beams of the LHC cross with a small angle at interaction points. In this study we used a crossing angle of 300 μrad which is an optimized value when both beam-beam effects and triplet field errors are taken into account [14]. Because of the beam separation, the higher-order field errors in HGQ feed down to lower orders. Even though the skew quadrupole component of the field error in HGQ is not included, the linear coupling as well as tune shifts exist if there is no linear correction in the ring. In the test lattice we used twelve normal quadrupoles and eight skew quadrupoles in eight outer triplets of the LHC to tune and to match the lattice functions, and to achieve a full decoupling at two high luminosity IRs. All insertions are perfectly matched to the arc sections. The fractional parts of horizontal and vertical tunes are $\nu_x = 0.31$ and $\nu_y = 0.32$, respectively.

The fifth-order IPF map was constructed from the fifth-order one-turn Taylor map of the LHC at the high luminosity interaction point. To test the IPF map, the dynamic aperture

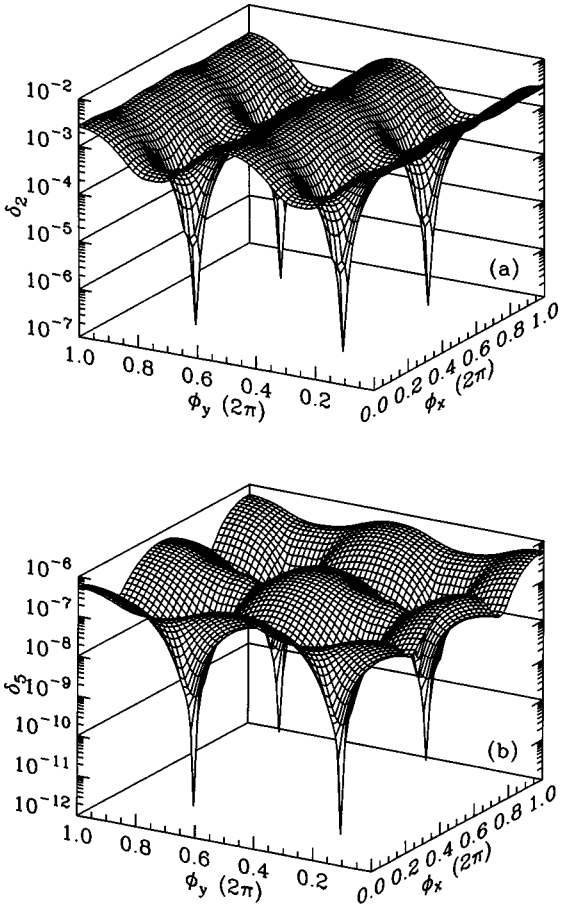

FIG. 4. Accuracy of (a) the second-order IPF map and (b) the fifth-order IPF map of the four-dimensional Hénon map. ϕ_x and ϕ_y are phase-space angle variables and $I_x = I_y = 0.1$. $\nu_x = 0.2114$ and $\nu_y = 0.2314$.

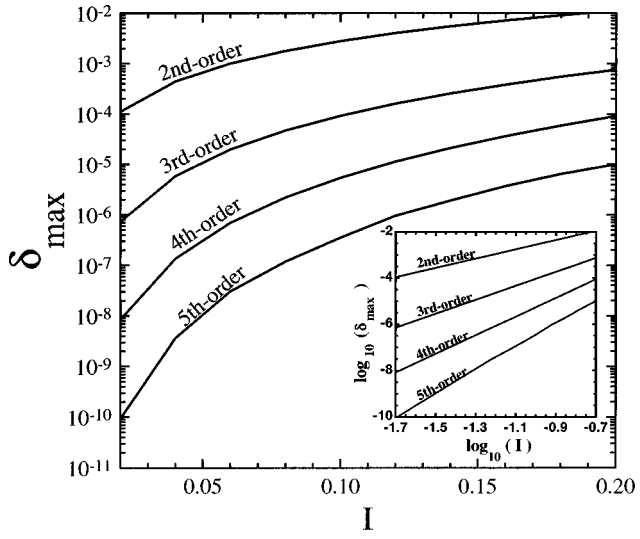

FIG. 5. The maximal relative error $\delta_{\max}$ of the IPF approximation of the four-dimensional Hénon map is plotted as a function of phase-space amplitude I. The number on each curve indicates the order of the IPF map. The inset plots $\log_{10}(\delta_{\max})$ as a function of $\log_{10}(I)$. $\nu_x = 0.2114$ and $\nu_y = 0.2314$.

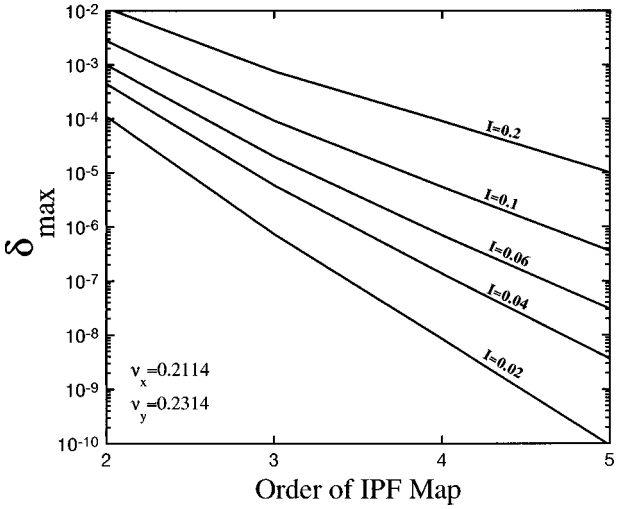

FIG. 6. The maximal relative error $\delta_{\max}$ of the IPF approximation of the four-dimensional Hénon map is plotted as a function of the order of the IPF map. The number on each curve indicates phase-space amplitude $I_x = I_y = I$. $\nu_x = 0.2114$ and $\nu_y = 0.2314$.

was calculated with 10^5-turn tracking by using both the IPF map and element-by-element tracking. Tracking of particle motions has been done without synchrotron oscillations and momentum deviations. To improve the statistical significance of the simulations, we have used 50 different samples of random multiple components generated with different seed numbers in a random number generator routine.

Figure 7 plots the dynamic aperture (DA) calculated by using the fifth-order IPF map versus DA calculated by element-by-element tracking for 50 random samples, which shows a very good agreement between these two methods. With element-by-element tracking, the smallest and average DA of the 50 samples are found to be 7.2σ and 14.7σ, respectively, where σ is the transverse beam size. At the high luminosity interaction points, $\sigma = 15.9$ μm [13]. On the other hand, the smallest and average DA obtained by using the IPF map are 7.6σ and 15.3σ, respectively. The IPF map,

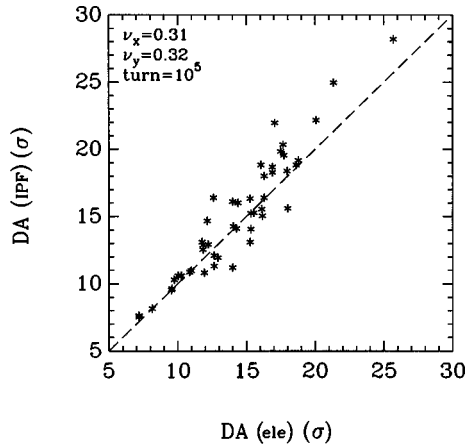

FIG. 7. The dynamic aperture [DA (IPF)] of 50 random samples of the LHC collision lattice calculated by using the fifth-order IPF map vs the dynamic aperture [DA (ele)] calculated by element-by-element tracking. The tracking turn is 10^5. $\nu_x = 0.31$ and $\nu_y = 0.32$. The unit of the dynamic aperture is the transverse beam size σ.

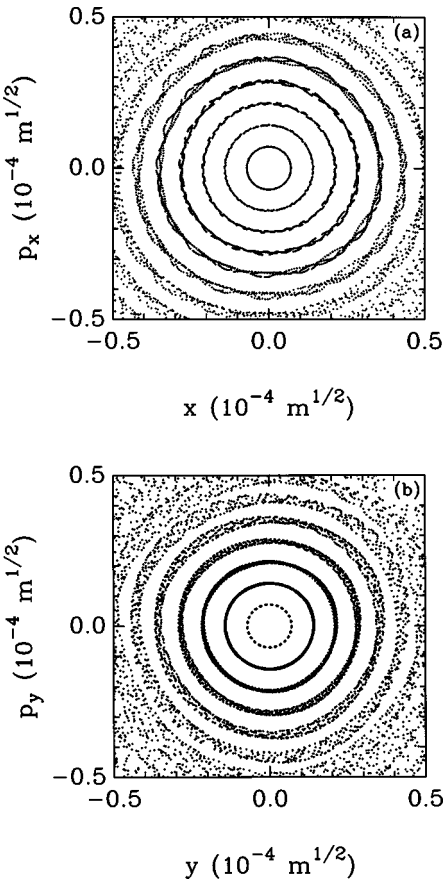

FIG. 8. Projection of normalized phase space on (a) x-p_x plane and (b) y-p_y plane of a typical random sample of the LHC collision lattice at the high luminosity interaction point. $\nu_x=0.31$ and $\nu_y=0.32$.

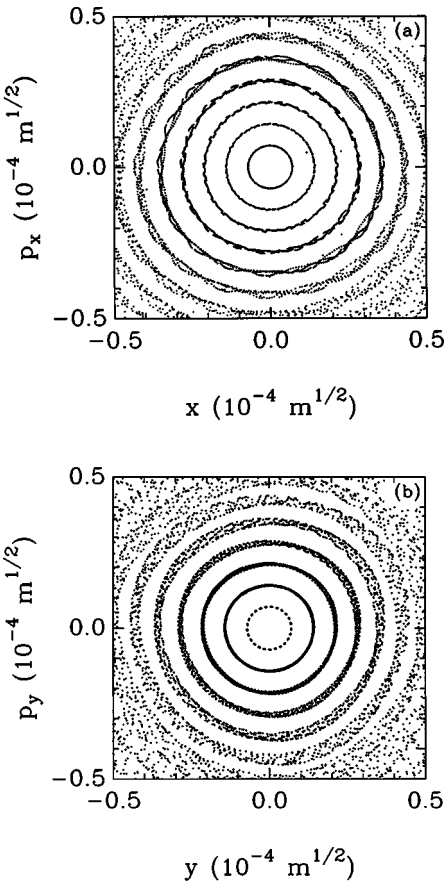

FIG. 9. Projection of normalized phase space on (a) x-p_x plane and (b) y-p_y plane of the fifth-order IPF map for the same case in Fig. 8.

therefore, accurately predicts the dynamic aperture.

To compare the detail of the phase space between the IPF map and the element-by-element tracking, we have also examined the difference in phase-space plots and calculated the errors in the IPF map by using Eqs. (6) and (7). Figures 8 and 9 plot the two-dimensional projections of the phase space of the LHC by using element-by-element tracking and by using the fifth-order IPF map, respectively, for a typical random sample. Comparison of Figs. 8 and 9 shows very little difference in the phase-space region of interest between the original system and its IPF map. In Fig. 10 the maximal relative error at a given phase-space amplitude $\delta_{\max}$ of the same sample is plotted as a function of I, which shows that the difference between the original system and its IPF approximation is very insignificant.

V. SUMMARY

For a nonlinear system, a valid symplectic-map approximation should contain a similar long-term behavior to that of the original system over the phase-space region of interest. In order to investigate such ''accuracy'' of the IPF map, a comparison study of the long-term behavior has been conducted with two examples: a four-dimensional Hénon map of which the IPF maps were constructed as approximations and the LHC collision lattice of which the IPF map was compared with element-by-element tracking. The maximal error of the nth-order IPF map at a given phase-space amplitude is found to be proportional to the $(n+1)$th power of the phase-space amplitude. Over the phase-space region of interest, a symplectic system can therefore be approximated by an IPF map with the desired accuracy. We have also examined the phase-space topology of the IPF maps by repeatedly applying the

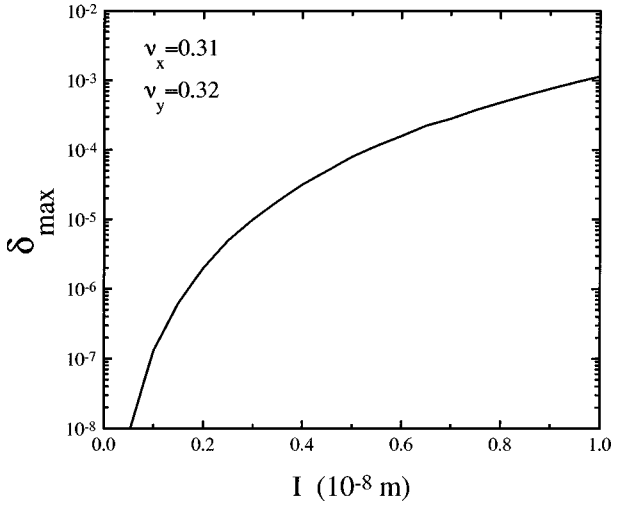

FIG. 10. The maximal relative error $\delta_{\max}$ of the fifth-order IPF map is plotted as a function of phase-space amplitude $I_x=I_y=I$ for the LHC collision lattice at the high luminosity interaction point. $\nu_x=0.31$ and $\nu_y=0.32$.

maps to various initial conditions. It was found that the IPF maps retain a similar resonance structure and have similar long-term behavior of the original system even in regions where the maps are quite nonlinear. The 10^5-turn tracking study has been conducted for the LHC collision lattice by using both the fifth-order IPF map and element-by-element tracking. The IPF map accurately predicts the same dynamic aperture as does element-by-element tracking. Our study suggests that the IPF map is a reliable model for the study of the long-term behavior of beam particles in large storage rings.

One remaining question for the application of the IPF map is the significance of the singularities in the IPF map [10]. The factorization bases of IPF are of the solutions of integrable Hamiltonian equations and they contain low-dimensional resonances. Near the hyperbolic points of those resonances, trajectories of the IPF map become highly unstable. Of systems we studied, those resonances are far away from the phase-space region of interest. It is, however, necessary to have a thorough understanding of any correlation between the resonances in the factorization bases and the resonances of the original system in order to understand any limitation of the IPF map. Such an understanding of the resonances could also enable one to use the map to easily get an idea of which resonances in the original system are potentially problematic for the stability of particle motion.

ACKNOWLEDGMENTS

This work is supported by the National Science Foundation under Grant No. PHY-9722513, and the University of Kansas General Research Fund.

[1] A. Dragt, in *Physics of High-Energy Particle Accelerators*, edited by R. A. Carrigan *et al.*, AIP Conf. Proc. No. 87 (AIP, New York, 1982).

[2] M. Berz, Part. Accel. **24**, 109 (1989).

[3] A. Dragt and J. Finn, J. Math. Phys. **17**, 2215 (1976).

[4] A. J. Dragt and D. T. Abell, ''Symplectic maps and computation of orbits in particle accelerators,'' University of Maryland report, 1995, and references herein.

[5] Y. T. Yan, *Physics of Particle Accelerators*, edited by M. Month and M. Diene, AIP Conf. Proc. No. 249 (AIP, New York, 1992), p. 378.

[6] Y. T. Yan, P. S. Channell, and M. J. Syphers, ''Performance of an algorithm for symplectic implicit one-turn map tracking,'' Superconducting Super Collider Laboratory Report No. SSCL-157, 1993.

[7] J. Irwin, in *Accelerator Physics at the Superconducting Super Collider*, edited by Y.T. Yan and J.P. Naples, AIP Conf. Proc. No. 326 (AIP, New York, 1995), p. 662.

[8] D. Abell, Ph.D. thesis, University of Maryland, 1995. (1995).

[9] J. Shi and Y. T. Yan, Phys. Rev. E **48**, 3943 (1993).

[10] J. Shi, Phys. Rev. E **50**, 532 (1994).

[11] J. Shi and Y.T. Yan, in *Accelerator Physics at the Superconducting Super Collider*, edited by Y.T. Yan and J.P. Naples, AIP Conf. Proc. No. 326 (AIP, New York, 1995), p. 678.

[12] The LHC Study Group, ''The Large Hadron Collider Conceptual Design,'' CERN Report No. CERN/AC/95-05(LHC), 1995.

[13] G. Sabbi *et al.*, in *Proceedings of the 1997 IEEE Particle Accelerator Conference* (IEEE, New York, 1998).

[14] W. Chou and D. Ritson, in *Proceedings of the 1997 IEEE Particle Accelerator Conference* (IEEE, New York, 1998).